Title page

A critical role for MSR1 in vesicular stomatitis virus infection of the central nervous system

Duomeng Yang[1], Tao Lin[1], Andrew G. Harrison[1], Tingting Geng[1], Huadong Wang[2], Penghua Wang[1*]

[1] Department of Immunology, School of Medicine, University of Connecticut Health Center, Farmington, CT 06030, USA

[2] Department of Pathophysiology, Key Laboratory of State Administration of Traditional Chinese Medicine of the People's Republic of China, School of Medicine, Jinan University, Guangzhou 510632, Guangdong, China

*Address correspondence to: Penghua Wang, Ph.D., Department of Immunology, School of Medicine, University of Connecticut Health Center, Farmington, CT 06030, USA. Email: pewang@uchc.edu, Tel: 860-679-6393

Running title: MSR1 is a cellular receptor for VSV

Abstract

Macrophage scavenger receptor 1 (MSR1) plays an important role in host defense to bacterial infections, M2 macrophage polarization and lipid homeostasis. However, its physiological function in viral pathogenesis remains poorly defined. Herein, we report that MSR1 facilitates vesicular stomatitis virus (VSV) infection in the spinal cord. Msr1-deficient (*Msr1*$^{-/-}$) mice presented reduced morbidity and mortality following lethal VSV infection, along with normal viremia and antiviral innate immune responses, compared to *Msr1*$^{+/-}$ littermates and wild-type mice. Msr1 expression was selectively upregulated in the spinal cord, which was the predominant target of VSV infection. The viral load in the spinal cord was positively correlated with Msr1 expression level and was reduced in *Msr1*$^{-/-}$ mice. Through its extracellular domain, MSR1 interacted with VSV surface glycoprotein and facilitated its cellular entry. In conclusion, our results demonstrate that MSR1 serves as a cellular entry receptor for VSV and facilitates its infection specifically in the spinal cord.

Key words: vesicular stomatitis virus, MSR1, scavenger receptor.

42 **Introduction**

43 Macrophage scavenger receptor 1 (MSR1; also known as CD204, SCARA1 and SR-A1), a
44 member of Class A scavenger receptors, performs many functions in homeostasis and
45 immunity, including pathogen clearance, lipid metabolism and macrophage polarization (1).
46 MSR1 recognizes a wide range of ligands including oxidized low-density lipoprotein
47 (oxLDL), endogenous proteins, beta-amyloid, lipoteichoic acid (LTA) and bacterial
48 lipopolysaccharide (LPS) (2, 3). The ligand promiscuity of MSR1 is probably due to its
49 function as a component of other pathogen pattern recognition receptor (PRR) signaling
50 complexes. For instance, MSR1 interacts with receptor tyrosine kinase MER (MERTK) to
51 enable apoptotic cell clearance (4). MSR1 partners with TLR4 to sense LPS that leads to
52 activation of nuclear factor-κB (NF-κB) signaling (5), and therefore contributes to either a
53 pro- or anti-inflammatory responses in Alzheimer's disease, sepsis, cancer and atherosclerosis
54 conditions (6-8). MSR1 recognizes and internalizes dead cells or debris through interaction
55 with spectrin in macrophages (9). MSR1 also promotes M2 macrophage polarization and Th2
56 cell responses to bacterial infection by suppressing nuclear translocation of interferon
57 regulatory factor 5 (IRF5) (10). The functions of MSR1 during viral infection may vary with
58 virus species and disease conditions. MSR1 signaling may protect mice against lethal herpes
59 simplex virus infection (11), activate autophagy to control Chikungunya virus infection (12)
60 and limit replication-defective adenovirus type 5-elicited hepatic inflammation and fibrosis
61 by promoting M2 macrophage polarization (13). MSR1 appears to function as a carrier of
62 extracellular dsRNA of hepatitis C virus and present it to endosomal TLR3 and cytoplasmic
63 RIG-I like receptors, resulting in an antiviral type I IFN response (14, 15). However, MSR1

signaling could aggravate the pathogenesis of murine hepatitis virus-induced fulminant hepatitis by enhancing neutrophil NETosis formation-induced complement activation (16).

Vesicular stomatitis virus (VSV) is a negative-sense, single-stranded RNA virus of the *Rhabdoviridae* family. This bullet-shaped virus infects a wide range of cells through its surface glycoprotein (VSV-G) (17, 18). Although VSV infection in humans is rare and very mild, it is common in livestock (e.g. cattle, horses and swine) and may produce significant economic losses, particularly in the southwestern states of the Unites States (19). Because of its broad cell tropism, easily genetic engineering and lack of preexisting human immunity against it, VSV is widely used as a model virus for fundamental research and vaccine development (20, 21). Like rabies virus, VSV is a neurotropic virus that primarily infects animals and occasionally humans (22-24). However, although there are decades of research on the mechanism of VSV neurotropism, the effects of animal model, route of inoculation, and the many signaling pathways that affect VSV neurotropism raise many unanswered questions about the mechanisms involved in neurovirulence. Herein, we report that Msr1 facilitates VSV infection in the spinal cord specifically. Msr1 serves as a cellular receptor that is selectively and highly upregulated in the spinal cord following VSV infection. Msr1-deficiency thus renders mice resistant to lethal VSV infection.

Results

Msr1 contributes to VSV pathogenesis in mice

MSR1 plays an important role in host defense to microbial infections (1). However, its physiological function in viral pathogenesis may vary significantly with viral species. We

86 investigate this using VSV, a model RNA virus for the study of innate antiviral immune
87 responses. Msr1 mRNA was expressed in various tissues with the highest in spleen (Fig. 1a).
88 We then infected *Msr1*$^{-/-}$ and wild-type (WT, C57BL/6) control mice with a lethal dose of
89 VSV. Intriguingly, ~90% of the WT mice (n=12) succumbed to VSV infection, but only ~30%
90 *Msr1*$^{-/-}$ mice died (n=12) (Fig. 1b). The overall survival rate of *Msr1*$^{-/-}$ mice was much higher
91 than that of WT mice (*P*=0.001, Log-Rank test). In addition, the disease severity of WT mice
92 was continuously increased from day 4 after infection and much greater than *Msr1*$^{-/-}$ mice
93 (Fig. 1b). Almost all infected WT mice developed severe symptoms such as hind-limb
94 paralysis as well as decreased mobility (Fig. 1c). To validate the phenotypic results, we
95 produced *Msr1*$^{-/-}$ and *Msr1*$^{-/+}$ littermates and repeated VSV infection. We confirmed that Msr1
96 protein level in *Msr1*$^{+/-}$ was the same as that in WT bone marrow-derived macrophages
97 (BMDM), which express abundant Msr1 (Fig. 1d). Consistently, the survival rate and disease
98 score of *Msr1*$^{+/-}$ mice infected with VSV were similar with WT mice. ~ 80% of infected
99 *Msr1*$^{+/-}$ mice (n=6) presented severe hind-limb paralysis and succumbed to lethal VSV
100 infection, while none of *Msr1*$^{-/-}$ mice (n=6) showed severe symptoms (Fig. 1e). These data
101 suggest that Msr1 contributes to the pathogenesis of VSV-induced disease.

102 Msr1 plays an important role in the maintenance of immune homeostasis and is reported
103 to aggravate virus-induced fulminate hepatitis pathogenesis by mediating C5a-induced
104 proinflammatory response(16). We thus assessed VSV viremia and the serum levels of type I
105 IFN and inflammatory cytokines between VSV-infected WT, *Msr1*$^{+/-}$ and *Msr1*$^{-/-}$ littermates
106 by multiplex ELISA and quantitative RT-PCR. Interestingly, the viremia and cytokine levels
107 (i.e. IFN-α, IFN-γ, TNF-α, IL-10, CXCL-10, IL-1β) in *Msr1*$^{-/-}$ mice were similar to WT and

108 *Msr1*$^{+/-}$ littermates (Fig. 2a, b, Fig. S1a, b). These results demonstrate that Msr1 is
109 dispensable for systemic VSV dissemination and innate immune responses.

110 **Msr1 is critical for VSV infection in the spinal cord**

111 VSV shows a strong neurotropism and causes severe neurological disorders in a variety of
112 rodent and primate animals though the underlying mechanism remains elusive (25). Indeed,
113 we observed overt hind-limb paralysis and immobility in WT mice (Fig. 1b-e), indicative of
114 severe infection in the central nervous system (CNS). We therefore evaluated viral loads in
115 different tissues after VSV infection. As shown in Fig. 3a, the VSV load in the spinal cord
116 was much higher than other tissues in VSV-infected *Msr1*$^{+/-}$ mice. Then, we examined the
117 CNS specimens from VSV-infected *Msr1*$^{+/-}$ and *Msr1*$^{-/-}$ littermates. We found that the viral
118 load in the spinal cord of *Msr1*$^{-/-}$ mice was significantly lower than that of *Msr1*$^{+/-}$ mice, while
119 the difference in the brain was moderate (Fig. 3b-d). This result is consistent with
120 VSV-induced severe paraplegia, which is most often caused by spinal cord injury (26).
121 Interestingly, the *Msr1* expression was sharply induced by VSV in the spinal cord and
122 modestly in the liver, while decreased in the spleen after infection (Fig. 3e). A strong positive
123 correlation between *Msr1* expression level and VSV load in the spinal cord was noted; the
124 association was moderate in the brain and spleen (Fig. 3f), suggesting that Msr1 is a
125 determinant of VSV infection in the spinal cord.

126 The scavenger receptor family consists of 10 classes, which are structurally
127 heterogeneous with little or no homology (1). MSR1 belongs to the Class A receptors, which
128 all have a extracellular collagenous domain (1). The aforementioned results suggest that
129 MSR1 is upregulated by VSV specifically in the spinal cord. We then asked if other members

130 of Class A and B may be induced similarly by VSV. The results show that *CD36* (*Scarb3*)
131 was also markedly induced in the spinal cord after VSV infection (Fig. 3g), but none of the
132 Class A/B scavenger receptors tested were significantly changed in the expression levels in
133 the infected brain (Fig. 3h). The LDL receptor family members serve as the cellular receptors
134 for VSV (27), and are also expressed in the nervous system (28); we thus examined the
135 expression of *Ldlr* in the brain and spinal cord. Intriguingly, *Ldlr* expression was higher in the
136 spinal cord than brain, but not significantly changed after VSV infection in either tissue (Fig.
137 3i). These findings suggest that Msr1 is critical for VSV infection, specifically in the spinal
138 cord.
139

140 **Msr1 mediates cellular entry of VSV**

141 The above-mentioned data suggest that MSR1 may facilitate VSV infection directly. Of note,
142 MSR1 is known to recognize a wide range of self- and microbial ligands, in particular,
143 oxidized low density lipoproteins(2, 3). We thus hypothesized that MSR1 could mediate
144 cellular entry of VSV. To this end, we employed primary neuron culturing from neonatal
145 *Msr1*$^{+/-}$ and *Msr1*$^{-/-}$ littermates and BMDM which express abundant Msr1 (Fig. 4c). Indeed,
146 the VSV load in *Msr1*$^{-/-}$ neurons (Fig. 4a) and the virus titer in its culture medium (Fig. 4b)
147 were significantly decreased compared to *Msr1*$^{+/-}$ littermates. The intracellular VSV-G
148 protein level and extracellular infectious virions in *Msr1*$^{-/-}$ BMDMs were much lower than
149 those in WT cells (Fig. 4d-f). We next determined if cellular entry of VSV was impaired in
150 *Msr1*$^{-/-}$ cells. BMDMs were inoculated with VSV at 4 °C for 2hrs to allow for VSV
151 attachment to the cell surface, at 37 °C for 30 min to allow for VSV entry into cells, and

152 lastly were washed extensively to remove unbound virions. Indeed, there were fewer VSV
153 virions attached to *Msr1*$^{-/-}$ than WT cells at 4 °C and consequently fewer virions inside
154 *Msr1*$^{-/-}$ cells at 37 °C (Fig. 4g). These data show that Msr1 mediates cellular entry of VSV.

155 Human MSR1 protein shares 70% identity and 81% similarity with mouse Msr1. We
156 then asked if the function of MSR1during VSV infection is evolutionarily conserved. To this
157 end, we evaluated VSV infection in a human *MSR1*$^{-/-}$ trophoblast line that was generated
158 recently in our hands (12). Indeed, VSV-G protein level in *MSR1*$^{-/-}$ trophoblasts was much
159 less than that in WT cells at 12 hrs after VSV infection (Fig. 5a). Consistently, the
160 fluorescence intensity of VSV-GFP in *MSR1*$^{-/-}$ trophoblasts was also decreased compared to
161 WT cells (Fig. 5b), and the plaque assay further showed a significant reduction in VSV
162 virions in the culture medium of *MSR1*$^{-/-}$ compared to WT trophoblasts (Fig. 5c).
163 Overexpression of MSR1 significantly increased VSV-G protein level (Fig. 5d), VSV-GFP
164 fluorescence intensity (Fig. 5e), and VSV titer in the cell culture medium (Fig. 5f), compared
165 to the vector control. Epichromosomal complementation of MSR1 gene in *MSR1*$^{-/-}$
166 trophoblasts restored VSV infection (Fig. 5g).

167 MSR1 is a cell surface protein with a short intracellular N-terminus, a transmembrane
168 domain and a long extracellular portion. We postulated that the extracellular portion mediates
169 VSV entry. To prove this, we dissected MSR1 into several fragments: amino residues 1-50
170 (cytoplasmic N-tail), 1-80 (cytoplasmic N-tail plus transmembrane), and 51-end
171 (extracellular domains with transmembrane), expressed them in trophoblasts (Fig. 5h, Fig.
172 S2a) and infected cells with VSV-GFP for 12 hrs. Intriguingly, both the fragment (51-end)
173 and full-length (1-end) MSR1 enhanced VSV-G protein level and VSV-GFP fluorescence

174 intensity; while the fragments without the extracellular domains (1-50 and 1-80) failed to do
175 so (Fig. 5i, j). These results demonstrate that MSR1 facilitates cellular entry of VSV through
176 its extracellular domain.

177 **MSR1 interacts with VSV glycoprotein G via its extracellular domain**

178 Based on the aforementioned data, we hypothesized that MSR1 serves as a cellular receptor
179 for VSV. We thus employed an immunoprecipitation assay to investigate if MSR1 full-length
180 (1-end) and/or fragments (1-80, 51-end, respectively) directly interact with intact VSV-GFP
181 virions. In agreement with Fig. 5h-j, both the 51-end and full-length of MSR1 pulled-down
182 infectious virions; while the MSR1 (1-80) did not (Fig. 6a-c). Of note, with considerably less
183 protein expression, the 51-end fragment pulled down the same amount of VSV-GFP as
184 full-length MSR1 (Fig. 6a-c), suggesting that the extracellular fragment mediates MSR1
185 binding to VSV virions. We further asked if MSR1 directly interacts with VSV surface
186 glycoprotein G that mediates VSV entry into host cells. We performed co-transfection of
187 VSV-G and FLAG-MSR1/fragment plasmids into HEK293 cells and immunoprecipitation
188 using an anti-FLAG antibody. The results show that the fragment (51-end) and full-length
189 (1-end) FLAG-MSR1 pulled down VSV-G, while the empty vector and the fragment 1-80 did
190 not (Fig. 6d).

191

192 **Discussion**

193 Although MSR1 has proven to perform a variety of functions in homeostasis and host
194 immunity due to its ability to recognize a diverse range of ligands (2, 3), its role in viral
195 pathogenesis remains poorly defined. MSR1 signaling may be protective against

196 Chikungunya virus and herpes simplex virus infection (11, 12), but could also contribute to
197 hepatitis virus-induced liver damage (16). In this study, our data collectively demonstrate that
198 MSR1 serves as a cellular receptor facilitating VSV infection specifically in the spinal cord,
199 and this is substantiated by several lines of experimental evidence. Firstly, Msr1-deficient
200 mice were strikingly resistant to VSV-elicited hind-limb paralysis compared to their
201 wild-type littermates. However, Msr1 was dispensable for systemic VSV dissemination and
202 innate immune responses. Secondly, the viral load in the spinal cord was the highest and the
203 fold induction of Msr1 expression by VSV was the greatest among all tested tissues. Of note,
204 the Msr1 expression level was positively correlated with VSV load in the spinal cord. These
205 results not only demonstrate a strong tropism of VSV for the spinal cord that leads to severe
206 paraplegia(26),(25), but also reveal a novel function for Msr1 as a critical determinant of
207 VSV infection specifically in the spinal cord. Thirdly, VSV attachment, entry, and
208 consequently replication was significantly reduced in both mouse primary *Msr1*$^{-/-}$
209 macrophages and human *MSR1*$^{-/-}$ trophoblasts. While overexpression of MSR1 could enhance
210 cellular entry of VSV and subsequent replication. Lastly, MSR1, through its extracellular
211 domain, interacted with VSV virions through its surface glycoprotein G and overexpression
212 of the extracellular section alone was sufficient to promote VSV infection. These
213 observations suggest that MSR1 is an entry receptor for VSV (17, 18).

214 To date, the membrane lipid phosphatidylserine and endoplasmic reticulum chaperone
215 Gp96 are important for VSV entry, but not as a receptor (25). The LDL receptor and its
216 family members were recently characterized as entry receptors for VSV in both human and
217 mouse cells (27). The widespread expression pattern of the LDLR family members may thus

218 in part underlie VSV pantropism. However, the *Rhabdoviridae* viruses (e.g. rabies virus, VSV)
219 specifically invade and replicate in motor neurons that exist predominately in the spinal cord
220 (29), and subsequent retrograde or anterograde spread of progeny virions in the motor nerve
221 system results in paraplegia (30, 31). Indeed, this study demonstrates that VSV primarily
222 targets the spinal cord, and secondarily the brain. Intriguingly MSR1 is essential for VSV
223 infection only in the spinal cord. In agreement with this, among all tested Class A and B
224 scavenger receptors, MSR1 is the most significantly upregulated member in the spinal cord;
225 while LDLR expression is unchanged following VSV infection. These observations suggest
226 that MSR1 becomes important for VSV infection of the spinal cord at least partly because
227 MSR1 expression is robustly upregulated. On the other hand, MSR1 could contribute to
228 neuronal inflammation and apoptosis by activating NF-κB signaling pathway in the spinal
229 cord (32). However, our data do not necessarily rule out the importance of LDLR family to
230 VSV infection in the spinal cord. Indeed, LDLR expression in the spinal cord, either before
231 or after VSV infection, is much higher than the brain.

232 In sum, we herein define MSR1 as a cellular entry receptor for VSV infection
233 specifically in the spinal cord. MSR1 can be selectively and highly upregulated in the spinal
234 cord following VSV infection. Given that VSV and its pseudotyped viruses have been widely
235 applied to vaccine research and oncolytic therapy (33-35), it seems plausible to improve
236 VSV-mediated oncolytic efficacy by manipulating MSR1 expression.

237

238

239 **Materials and Methods**

240 *Animals*

241 All mice were purchased from the Jackson Laboratory and housed under the same conditions.
242 C57BL/6J mice (Stock No: 000664) were employed as the wild-type control mice. *Msr1*$^{-/-}$
243 mice (B6.Cg-*Msr1*^{tm1Csk}/J, stock No: 006096) were made from 129 embryonic stem (ES) cells
244 and then backcrossed to C57BL/6J mice for 12 generations. *Msr1*$^{+/-}$ mice were made by
245 backcrossing *Msr1*$^{-/-}$ mice to C57BL/6J mice. All of the gene-mutant and wild type mice were
246 normal in body weight and general health. Sex- and age-matched (6-8 weeks) mice were used
247 for all the experiments. The animal protocols were approved by the Institutional Animal Care
248 & Use Committee at University of Connecticut adhering to the National institutes of Health
249 recommendations for the care and use of laboratory animals.

250

251 *Antibodies and plasmids*

252 The rabbit anti-Actin (Cat # 8456) antibody was purchased from Cell Signaling Technology
253 (Danvers, MA 01923, USA). The mouse anti-FLAG (Cat# TA50011) and rabbit
254 anti-human/mouse MSR1 (Cat# TA336699) antibodies were from Origene (Rockville, MD
255 20850, USA). The mouse anti-human MSR1 (Cat# MAB2708) antibody was obtained from
256 R&D Systems (Minneapolis, MN 55413, USA). Then rabbit anti-VSV-G (Cat#V4888)
257 antibody and the anti-FLAG M2 magnetic beads (Clone M2, Cat# M8823) were from
258 Sigma-Aldrich (St. Louis, MO, USA). The human MSR1 (Cat# RC209609) were obtained
259 from Origene (Rockville, MD 20850, USA). Human MSR1 and its fragment 1-50, 1-80 and
260 51-end were amplified by PCR and inserted into pcDNA3.1 (Zeo)-FLAG vector. The primers

261 are listed in the Supplemental Table S1.

262

263 *Cell culture and viruses*

264 Vero cells (monkey kidney epithelial cells, # CCL-81), human trophoblasts HTR-8/SVneo
265 (#CRL-3271) and L929 (mouse fibroblast cells, # CCL-1) were purchased from American
266 Type Culture Collection (ATCC) (Manassas, VA20110, USA). *MSR1*$^{-/-}$ trophoblasts were
267 generated in our previous study (12). Vero cells were grown in Corning® DMEM
268 (Dulbecco's Modified Eagle's Medium) supplemented with 10% FBS and 1%
269 penicillin/streptomycin. Human trophoblasts were cultured in Corning® RPMI 1640 medium
270 supplemented with 10% fetal bovine serum and 1% penicillin/streptomycin. Bone
271 marrow-derived macrophages (BMDMs) were differentiated from femur bone-derived bone
272 marrows in L929 conditioned medium (RPMI1640, 20%FBS, 30% L929 culture medium and
273 1% penicillin/streptomycin) in 10-cm Petri-dishes at 37 °C, 5% CO_2 for 7 days. The BMDMs
274 were then seeded in culture plates and cultured in regular RPMI1640 medium overnight
275 before further treatment. MycoZap (Lonza) were used regularly to prevent mycoplasma
276 contamination. The vesicular stomatitis virus (VSV) used in this study was Indiana strain
277 described previously (36), and the green fluorescence protein (GFP) tagged VSV was made
278 from this VSV. These viruses were propagated in Vero cells.

279

280 *Primary neuron culture*

281 The primary neuron culturing was performed according to a previous method(37). The brain
282 of a 3-day old neonate was dissected dorsally under a microscope; the vascular tunic was

283 removed; and then the brain was washed in ice-cold DMEM medium. The brain was then
284 broken into pieces by pipetting up and down in 0.125% trypsin with DNAse I, and then
285 digested for 30min in a 37 °C water bath, vortexed every 10 min. Digestion of the brain was
286 terminated by 10% FBS+DMEM, filtered through a 70μm cell strainer (ThemoFisher brand).
287 The filtrate was centrifuged at 500 x g at 4 °C for 5min to pellet neurons. The neurons were
288 then plated in 0.0125% poly-L-lysine-coated culture plates (overnight at 37°C), and cultured
289 in neurobasal medium (Gibco, U.S) with 2% B27 supplement (Gibco, U.S) at 37 °C, 5% CO_2
290 for 5-6 days.
291
292 *Mouse infection and disease monitoring*
293 VSV stock [~10^8 plaque forming units (PFU/ml)] was diluted in sterile phosphate buffered
294 saline (PBS), and ~10^7 PFU was injected into mice retro-orbitally (38). The mice were
295 monitored for disease progression over a period of 8 days after infection. The main symptoms
296 were mobility and hind-limb paralysis. The severity of disease was measured using a scale
297 from 0 (no symptom), 1 (no plantar stepping in one hind leg), 2 (no plantar stepping in two
298 hind legs or slight ankle movement in one hind leg), 3 (slight ankle movement in two hind
299 legs or no ankle movement in one hind leg), 4 (no ankle movement in one hind leg and slight
300 in the other one) to 5 (no ankle movement in both hind legs, almost loss of all movement
301 ability), as described previously (26). The mice scored for 5 were euthanized as a humane
302 endpoint according to the animal protocol.
303
304 *Real-time reverse transcription PCR*

305 Animal tissues or whole blood (30µl) were collected in 330µl of lysis buffer (Invitrogen
306 RNAasy mini-prep kit). The heart, liver, lung, brain and spleen were minced with a pair of
307 scissors and homogenized in RLT buffer using an electrical pellet pestle (Kimble Chase LLC,
308 USA). RNA was extracted following the Invitrogen RNAasy mini-prep kit protocol, and
309 reverse-transcribed into cDNA using the TAKARA PrimeScriptTM RT Reagent Kit with
310 gDNA Eraser (Perfect Real Time) (#RR047A). qPCR was performed with gene-specific
311 primers and Bio-Rad SYBR Premix. qPCR results were calculated using the –ΔΔCt method
312 and beta actin gene as an internal control. The qPCR primers are summarized in supplemental
313 material Table S2.
314
315 *Plaque-forming assay*
316 The viral particles in tissue homogenates or cell culture medium were quantitated by plaque
317 forming assays as previously described (39). Briefly, samples were serially diluted by 10-fold
318 using DMEM without FBS, and then 500 µL of each diluted sample plus 500 µL DMEM
319 without FBS were added onto a Vero cell monolayer in a 6-well plate. The 6-well plate was
320 then incubated at 37 °C for 2 h. The inoculum was replaced with 1% SeaPlaque agarose (Cat#
321 50100, Lonza) in complete DMEM medium (2 ml). The plate was left at room temperature
322 for 30min to allow the agarose to solidify, and then moved to a cell culture incubator (37 °C,
323 5% CO_2). Plaques were visualized by a Neutral Red exclusion assay after 3 days.
324
325 *Western blotting assay*
326 Western blotting analysis was performed using standard procedures. Briefly, protein samples

327 were resolved by SDS-PAGE (sodium dodecyl sulfate-polyacrylamide gel electrophoresis)
328 and transferred to a nitrocellulose membrane. The membrane blot was incubated with a
329 primary antibody over night at 4 °C, washed briefly and incubated with a HRP-conjugated
330 secondary antibody for 1 hour at room temperature. An ultra-sensitive ECL substrate was
331 used for detection (ThermoFisher, Cat# 34095).
332
333 *Co-immunoprecipitation*
334 Trophoblasts or HEK293 cells were seeded at a density of $5x10^5$ cells/ml and transfected with
335 protein expression plasmids (pVSVG, 1-80, 51-end, 1-end of FLAG-MSR1, and vector)
336 using TransIT-X2® Transfection Reagent. Twenty-four hours after transfection, whole-cell
337 extracts were prepared from transfected trophoblasts in lysis buffer (150 mM NaCl, 50 mM
338 Tris pH 7.5, 1 mM EDTA, 0.5% NP40, 10% Glycerol) and were incubated with 50µl of
339 anti-FLAG magnetic beads for 2hrs at 4°C. The whole procedure of co-immunoprecipitation
340 was performed according to manufacturer's protocol (Anti-Flag Magnetic Beads,
341 Sigma-Aldrich). For co-immunoprecipitation of live VSV particles, $5x10^5$ cells/ml HEK293
342 cells were transfected with protein expression plasmids (1-80, 51-end, 1-end of FLAG-MSR1,
343 and vector). Twenty-four hours later, cells were lysed in lysis buffer and incubated with 50µl
344 of anti-FLAG magnetic beads for 2hrs at 4°C. The beads were washed three times with sterile
345 PBS to completely remove detergent and unbound cellular proteins, and were then incubated
346 with VSV-GFP virions (500µl, $1x10^7$ PFU/ml) for 2hrs at 4°C. The beads were washed with
347 sterile PBS three times to remove unbound virions and the bound virions were eluted with
348 3xFLAG peptide in sterile PBS. The VSV-GFP pulled down by FLAG-MSR1 and fragments

349 were then used to infect Vero cells or immunoblotting (Fig. S2b).

350

351 *Multiplex ELISA (enzyme-linked immunosorbent assay)*

352 BioLegend's LEGENDplex™ bead-based immunoassays of serum samples were performed
353 exactly according to the instruction of BioLegend's LEGENDplex™ kit. The flow cytometry
354 data were analyzed using the LEGENDplex™ data analysis software.

355

356 *Graphing and statistics*

357 The data from all experiments were analyzed using a Prism GraphPad Software and
358 expressed as mean ± S.D. Survival data were analyzed using a Log-rank (Mantel-Cox) test.
359 For *in vitro* cell culture results, a standard two-tailed unpaired Student's t-test was used. For
360 animal studies, an unpaired two-tailed nonparametric Mann-Whitney U test was applied to
361 statistical analysis. P values ≤ 0.05 were considered significant. The statistic statements of
362 experiments are detailed in each figure legend.

363

364

Acknowledgements

This work was supported by a National Institutes of Health grant R01AI132526 and UConn Health startup fund to P.W.

Author contributions

D.Y. designed and performed all the experimental procedures and data analyses. T.L., A.H., and T.G provided technical support and/or data analyses. H.W. assisted with data interpretation and discussion. P.W. conceived and oversaw the study. D.Y. and P.W. wrote the paper and all the authors reviewed and/or modified the manuscript.

Conflict of interest

The authors declare no competing financial/non-financial interest.

379 ## References

380 1. Canton J, Neculai D, Grinstein S. 2013. Scavenger receptors in homeostasis and immunity. Nat Rev
381 Immunol 13:621-34.
382 2. Pluddemann A, Mukhopadhyay S, Gordon S. 2011. Innate immunity to intracellular pathogens:
383 macrophage receptors and responses to microbial entry. Immunol Rev 240:11-24.
384 3. Pombinho R, Sousa S, Cabanes D. 2018. Scavenger Receptors: Promiscuous Players during Microbial
385 Pathogenesis. Crit Rev Microbiol 44:685-700.
386 4. Todt JC, Hu B, Curtis JL. 2008. The scavenger receptor SR-A I/II (CD204) signals via the receptor
387 tyrosine kinase Mertk during apoptotic cell uptake by murine macrophages. J Leukoc Biol 84:510-8.
388 5. Yu H, Ha T, Liu L, Wang X, Gao M, Kelley J, Kao R, Williams D, Li C. 2012. Scavenger receptor A (SR-A) is
389 required for LPS-induced TLR4 mediated NF-kappaB activation in macrophages. Biochim Biophys Acta
390 1823:1192-8.
391 6. Kelley JL, Ozment TR, Li C, Schweitzer JB, Williams DL. 2014. Scavenger receptor-A (CD204): a
392 two-edged sword in health and disease. Crit Rev Immunol 34:241-61.
393 7. Zhang Y, Wei Y, Jiang B, Chen L, Bai H, Zhu X, Li X, Zhang H, Yang Q, Ma J, Xu Y, Ben J, Christiani DC,
394 Chen Q. 2017. Scavenger Receptor A1 Prevents Metastasis of Non–Small Cell Lung Cancer via
395 Suppression of Macrophage Serum Amyloid A1. Cancer Research 77:1586.
396 8. Mukhopadhyay S, Varin A, Chen Y, Liu B, Tryggvason K, Gordon S. 2011. SR-A/MARCO-mediated ligand
397 delivery enhances intracellular TLR and NLR function, but ligand scavenging from cell surface limits
398 TLR4 response to pathogens. Blood 117:1319-28.
399 9. Cheng C, Hu Z, Cao L, Peng C, He Y. 2019. The scavenger receptor SCARA1 (CD204) recognizes dead
400 cells through spectrin. J Biol Chem 294:18881-18897.
401 10. Xu Z, Xu L, Li W, Jin X, Song X, Chen X, Zhu J, Zhou S, Li Y, Zhang W, Dong X, Yang X, Liu F, Bai H, Chen Q,
402 Su C. 2017. Innate scavenger receptor-A regulates adaptive T helper cell responses to pathogen
403 infection. Nat Commun 8:16035.
404 11. Suzuki H, Kurihara Y, Takeya M, Kamada N, Kataoka M, Jishage K, Ueda O, Sakaguchi H, Higashi T,
405 Suzuki T, Takashima Y, Kawabe Y, Cynshi O, Wada Y, Honda M, Kurihara H, Aburatani H, Doi T,
406 Matsumoto A, Azuma S, Noda T, Toyoda Y, Itakura H, Yazaki Y, Kodama T, et al. 1997. A role for
407 macrophage scavenger receptors in atherosclerosis and susceptibility to infection. Nature 386:292-6.
408 12. Yang L, Geng T, Yang G, Ma J, Wang L, Ketkhar H, Yang D, Lin T, Hwang J, Zhu S, Wang Y, Dai J, You F,
409 Cheng G, Vella A, Flavell RA, Fikrig E, Wang P. 2020. Macrophage scavenger receptor 1 controls
410 Chikungunya virus infection through autophagy. bioRxiv
411 doi:10.1101/2020.02.28.969832:2020.02.28.969832.
412 13. Labonte AC, Sung S-SJ, Jennelle LT, Dandekar AP, Hahn YS. 2017. Expression of scavenger receptor-AI
413 promotes alternative activation of murine macrophages to limit hepatic inflammation and fibrosis.
414 Hepatology (Baltimore, Md) 65:32-43.
415 14. DeWitte-Orr SJ, Collins SE, Bauer CM, Bowdish DM, Mossman KL. 2010. An accessory to the 'Trinity':
416 SR-As are essential pathogen sensors of extracellular dsRNA, mediating entry and leading to
417 subsequent type I IFN responses. PLoS Pathog 6:e1000829.
418 15. Dansako H, Yamane D, Welsch C, McGivern DR, Hu F, Kato N, Lemon SM. 2013. Class A scavenger
419 receptor 1 (MSR1) restricts hepatitis C virus replication by mediating toll-like receptor 3 recognition of
420 viral RNAs produced in neighboring cells. PLoS Pathog 9:e1003345.
421 16. Tang Y, Li H, Li J, Liu Y, Li Y, Zhou J, Zhou J, Lu X, Zhao W, Hou J, Wang XY, Chen Z, Zuo D. 2018.

422 Macrophage scavenger receptor 1 contributes to pathogenesis of fulminant hepatitis via
423 neutrophil-mediated complement activation. J Hepatol 68:733-743.
424 17. Ge P, Tsao J, Schein S, Green TJ, Luo M, Zhou ZH. 2010. Cryo-EM model of the bullet-shaped vesicular
425 stomatitis virus. Science 327:689-93.
426 18. Nikolic J, Belot L, Raux H, Legrand P. 2018. Structural basis for the recognition of LDL-receptor family
427 members by VSV glycoprotein. Nature communications 9:1029.
428 19. Rozo-Lopez P, Drolet BS, Londoño-Renteria B. 2018. Vesicular Stomatitis Virus Transmission: A
429 Comparison of Incriminated Vectors. Insects 9:190.
430 20. Bukreyev A, Skiadopoulos MH, Murphy BR, Collins PL. 2006. Nonsegmented negative-strand viruses as
431 vaccine vectors. J Virol 80:10293-306.
432 21. Mátrai J, Chuah MKL, VandenDriessche T. 2010. Recent advances in lentiviral vector development and
433 applications. Molecular therapy : the journal of the American Society of Gene Therapy 18:477-490.
434 22. Gagnidze K, Hajdarovic KH, Moskalenko M, Karatsoreos IN, McEwen BS, Bulloch K. 2016. Nuclear
435 receptor REV-ERBalpha mediates circadian sensitivity to mortality in murine vesicular stomatitis
436 virus-induced encephalitis. Proc Natl Acad Sci U S A 113:5730-5.
437 23. Quiroz E, Moreno N, Peralta PH, Tesh RB. 1988. A human case of encephalitis associated with vesicular
438 stomatitis virus (Indiana serotype) infection. Am J Trop Med Hyg 39:312-4.
439 24. Ludlow M, Kortekaas J, Herden C, Hoffmann B, Tappe D, Trebst C, Griffin DE, Brindle HE, Solomon T,
440 Brown AS, van Riel D, Wolthers KC, Pajkrt D, Wohlsein P, Martina BEE, Baumgartner W, Verjans GM,
441 Osterhaus A. 2016. Neurotropic virus infections as the cause of immediate and delayed
442 neuropathology. Acta Neuropathol 131:159-184.
443 25. Hastie E, Cataldi M, Marriott I, Grdzelishvili VZ. 2013. Understanding and altering cell tropism of
444 vesicular stomatitis virus. Virus Res 176:16-32.
445 26. Smith PD, Bell MT, Puskas F, Meng X, Cleveland JC, Jr., Weyant MJ, Fullerton DA, Reece TB. 2013.
446 Preservation of motor function after spinal cord ischemia and reperfusion injury through microglial
447 inhibition. Ann Thorac Surg 95:1647-53.
448 27. Finkelshtein D, Werman A, Novick D, Barak S, Rubinstein M. 2013. LDL receptor and its family
449 members serve as the cellular receptors for vesicular stomatitis virus. Proc Natl Acad Sci U S A
450 110:7306-11.
451 28. Beffert U, Stolt PC, Herz J. 2004. Functions of lipoprotein receptors in neurons. J Lipid Res 45:403-9.
452 29. Bradbury EJ, McMahon SB. 2006. Spinal cord repair strategies: why do they work? Nat Rev Neurosci
453 7:644-53.
454 30. Beier KT, Saunders A, Oldenburg IA, Miyamichi K, Akhtar N, Luo L, Whelan SP, Sabatini B, Cepko CL.
455 2011. Anterograde or retrograde transsynaptic labeling of CNS neurons with vesicular stomatitis virus
456 vectors. Proc Natl Acad Sci U S A 108:15414-9.
457 31. Koyuncu OO, Hogue IB, Enquist LW. 2013. Virus infections in the nervous system. Cell host & microbe
458 13:379-393.
459 32. Kong FQ, Zhao SJ, Sun P, Liu H, Jie J, Xu T, Xu AD, Yang YQ, Zhu Y, Chen J, Zhou Z, Qian DF, Gu CJ, Chen Q,
460 Yin GY, Zhang HW, Fan J. 2020. Macrophage MSR1 promotes the formation of foamy macrophage and
461 neuronal apoptosis after spinal cord injury. J Neuroinflammation 17:62.
462 33. Felt SA, Grdzelishvili VZ. 2017. Recent advances in vesicular stomatitis virus-based oncolytic
463 virotherapy: a 5-year update. The Journal of general virology 98:2895-2911.
464 34. Liang M, Yan M, Lu Y, Chen IS. 2013. Retargeting vesicular stomatitis virus glycoprotein pseudotyped
465 lentiviral vectors with enhanced stability by in situ synthesized polymer shell. Hum Gene Ther

466 Methods 24:11-8.
467 35. Lin K, Zhong X, Ying M, Li L, Tao S, Zhu X, He X, Xu F. 2020. A mutant vesicular stomatitis virus with
468 reduced cytotoxicity and enhanced anterograde trans-synaptic efficiency. Mol Brain 13:45.
469 36. You F, Wang P, Yang L, Yang G, Zhao YO, Qian F, Walker W, Sutton R, Montgomery R, Lin R, Iwasaki A,
470 Fikrig E. 2013. ELF4 is critical for induction of type I interferon and the host antiviral response. Nat
471 Immunol 14:1237-46.
472 37. Beaudoin GM, 3rd, Lee SH, Singh D, Yuan Y, Ng YG, Reichardt LF, Arikkath J. 2012. Culturing pyramidal
473 neurons from the early postnatal mouse hippocampus and cortex. Nat Protoc 7:1741-54.
474 38. Yardeni T, Eckhaus M, Morris HD, Huizing M, Hoogstraten-Miller S. 2011. Retro-orbital injections in
475 mice. Lab animal 40:155-160.
476 39. Wang P. 2016. Exploration of West Nile Virus Infection in Mouse Models. Methods Mol Biol
477 1435:71-81.
478
479
480
481

482 **Figure legends**

483

484 **Fig. 1 Msr1 contributes to VSV pathogenesis in mice**. **a)** *Msr1* mRNA expression in
485 various tissues of wild-type (WT, C57BL/6) and *Msr1*$^{-/-}$ mice, N=3 mice per genotype. **b)** The
486 survival curves and disease scores of WT and *Msr1*$^{-/-}$ mice challenged with 1×10^7
487 plaque-forming units (PFU) per mouse of VSV by retro-orbital injection, N=12
488 mice/genotype. P=0.001 (log-rank test), * P<0.05; ** P<0.01; *** P<0.001; **** P<0.0001,
489 non-parametric Mann-Whitney U test. **c)** The WT mice with paralyzed hind-limbs at day 6
490 post infection. **d)** Immunoblots of Msr1 protein expression in bone marrow-derived
491 macrophages (BMDM) of WT, *Msr1*$^{-/-}$ and *Msr1*$^{-/+}$ littermates. Beta Actin (Actb) is a
492 housekeeping control. **e)** The survival curves and disease scores of *Msr1*$^{-/-}$ and *Msr1*$^{-/+}$
493 littermates challenged with 1×10^7 PFU/mouse of VSV by retro-orbital injection, N=6
494 mice/genotype. All the error bars: mean ± S.E.M.

495

496 **Fig. 2 Msr1 is dispensable for systemic VSV dissemination and innate immune**
497 **responses**. **a)** The viral load in whole blood of WT mice, *Msr1*$^{+/-}$ and *Msr1*$^{-/-}$ littermates
498 infected with VSV, assessed by quantitative RT-PCR, N=6 mice/genotype. **b)** The serum
499 levels of type I IFN and inflammatory cytokines in *Msr1*$^{+/-}$ and *Msr1*$^{-/-}$ littermates after VSV
500 infection, assessed by multiplex ELISA, N=6 mice/genotype. All the data are presented as
501 mean ± S.E.M. and statistical significance are analyzed by non-parametric Mann-Whitney U
502 test.

503

504 **Fig. 3 Msr1 is critical for VSV infection specifically in the spinal cord**. Quantitative
505 RT-PCR analyses of VSV loads in **a)** different tissues of *Msr1*$^{+/-}$ mice (N=3 mice per group),
506 **b)** the spinal cords and **c)** the brains of *Msr1*$^{+/-}$ and *Msr1*$^{-/-}$ littermates on day 6 after infection
507 (N=6 mice/genotype). **d)** The VSV titers in the spinal cord and brain of *Msr1*$^{+/-}$ and *Msr1*$^{-/-}$
508 littermates on day 6 after infection, as assessed by plaque forming assay. N=6 mice/genotype.
509 **e)** Msr1 mRNA expression in different tissues of mock and VSV-infected mice on day 6 after
510 infection, N=3 mice per group. **f)** Correlation between *Msr1* expression and VSV load in
511 various tissues after VSV infection, N=3 mice per group. The mRNA expression of Class A
512 and B scavenger receptors in **g)** the spinal cord and **h)** the brain on day 6 after VSV infection,
513 as assessed by quantitative RT-PCR, N=3 mice per group. **i)** *Ldlr* mRNA expression in the
514 brain and spinal cord, N=3 mice per group. Mock: no virus. All the data are presented as
515 mean ± S.E.M. and statistical significances are analyzed by non-parametric Mann-Whitney U
516 test, * $P<0.05$, ** $P<0.01$.
517
518 **Fig. 4 Msr1 mediates cellular entry of VSV in primary mouse cells**. VSV loads in primary
519 neurons of *Msr1*$^{+/-}$ and *Msr1*$^{-/-}$ littermates at 36 h after inoculation (multiplicity of infection
520 =3), as assessed by **a)** quantitative RT-PCR and **b)** plaque forming assay. Each dot represents
521 an individual mouse. **c)** Immunoblots of Msr1 protein expression in WT and *Msr1*$^{-/-}$ bone
522 marrow-derived macrophages (BMDM) and peritoneal macrophages (PM). **d)** VSV-G
523 protein expression in BMDM, **e)** virus titer in culture medium and **f)** VSV-GFP fluorescence
524 under microscopy in BMDM at 48 h after VSV infection, N=3 biological replicates.
525 Objective: 20x, Scale bar: 100 μm. **g)** Quantitative RT-PCR analyses of VSV virions attached

526 to BMDM (4°C for 2 h) and entry into BMDM (37°C for 30 min), N=3 biological replicates.
527 Beta Actin (Actb) is a housekeeping control. Mock: no virus. All the data are presented as
528 mean ± S.E.M. and statistical significances are analyzed by a standard two-tailed unpaired
529 Student's t-test, * $P<0.05$, ** $P<0.01$.
530
531 **Fig. 5 MSR1 facilitates cellular entry of VSV through its extracellular domain**. **a)-c)** WT
532 and *MSR1*$^{-/-}$ trophoblasts were examined at 12 h post VSV-GFP inoculation, **a)** Immunoblots
533 of VSV-G protein level, **b)** VSV-GFP fluorescence intensity and **c)** VSV titers in the cell
534 culture medium, MOI=0.5. N=3 biological replicates. **d)-f)** WT and MSR1-overexpressed
535 trophoblasts were examined at 12 h post VSV-GFP inoculation, **d)** MSR1 protein expression,
536 VSV-G protein level, **e)** VSV-GFP fluorescence intensity and **f)** VSV titers in the culture
537 medium, MOI=0.5. N=3 biological replicates. The VSV-GFP fluorescence intensity in **b)** and
538 **e)** was calculated from 9 random fields of view from three biological replicates. Objective: 4x
539 (top) and 20x, Scale bar: 100 μm. **g)** Immunoblots of VSV-G protein level in *MSR1*$^{-/-}$
540 trophoblasts with epichromosomal complementation of an empty vector or FLAG-MSR1
541 expression plasmid at 12 h after VSV infection, MOI=0.5. **h)** The protein expression of
542 different FLAG-tagged MSR1 fragments at 24 h after transfection of plasmids in trophoblasts.
543 IB: immunoblotting. Amino residues 1-50 (cytoplasmic N-tail), 1-80 (cytoplasmic N-tail plus
544 transmembrane), 51-end (extracellular domains with transmembrane), and 1-end (full-length).
545 **i)** VSV-G protein level and **j)** VSV-GFP fluorescence intensity in the trophoblasts
546 overexpressing FLAG-MSR1 fragments at 12 h after VSV-GFP infection, MOI=0.5, N=3
547 biological replicates. Beta Actin (ACTB) is a housekeeping control. Mock: no virus. All the

548 data are presented as mean ± S.E.M. and statistical significances are analyzed by a standard
549 two-tailed unpaired Student's t-test, ** $P<0.01$, *** $P<0.001$, **** $P<0.0001$.
550
551 **Fig. 6 MSR1 interacts with VSV glycoprotein G via its extracellular domains**. **a-c)**
552 Binding of MSR1 to VSV virions. FLAG-MSR1 (human, 1-end) and its fragments (aa1-80,
553 51-end) were expressed in HEK293 cells and immunoprecipitated (IP) using anti-FLAG
554 antibody-coated magnetic beads, which were then incubated with intact VSV-GFP virions (4°C
555 for 2 h). The bound virions were eluted for **a)** immunoblotting (IB) with a mouse monoclonal
556 anti-FLAG and rabbit anti-VSV-G antibody, **b-c**) for re-infection in Vero cells for 12 h
557 followed by detection of **b)** VSV-GFP by fluorescence microscopy and **c)** VSV-G protein
558 level by immunoblotting. Mock: no virion. **d)** co-IP of FLAG-MSR1 and its fragments with
559 VSV-G in HEK293 cells transfected with expression plasmids. WCL: whole cell lysate.
560 Arrows point to the faint protein bands.
561
562
563
564
565
566
567
568
569
570
571
572
573
574
575
576

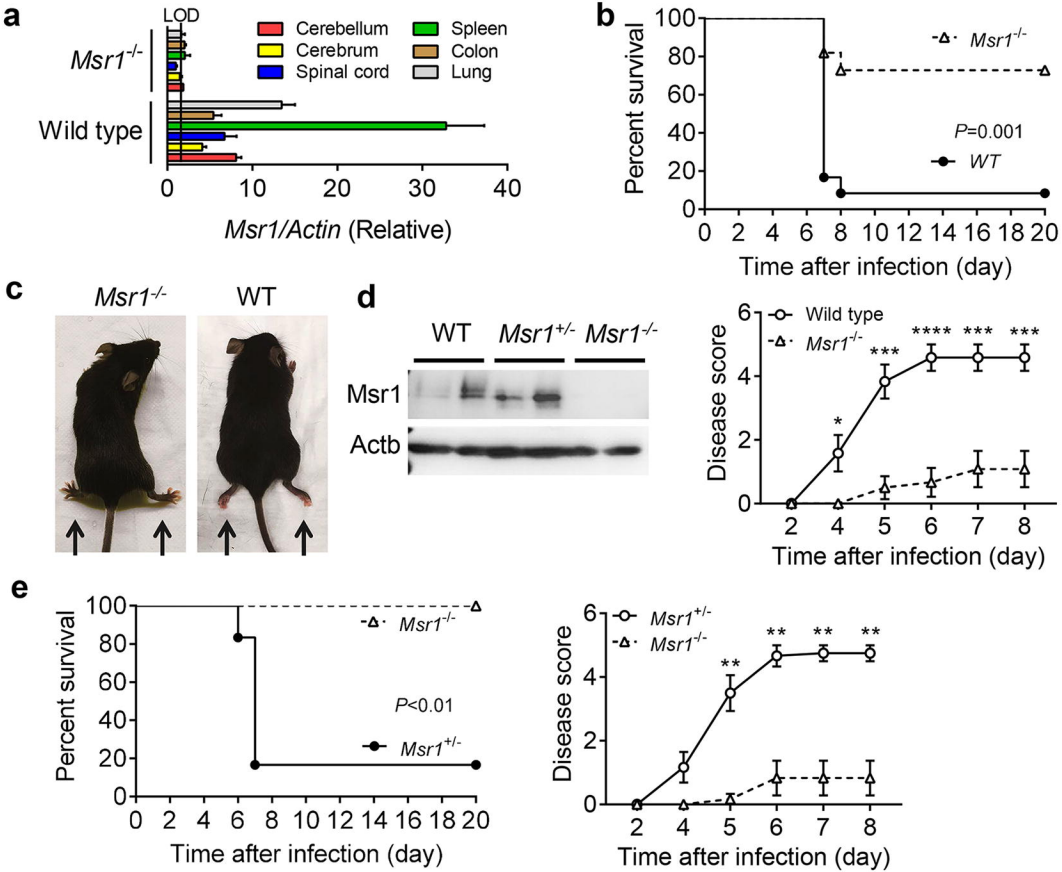
a
LOD
Cerebellum
Cerebrum
Spinal cord
Spleen
Colon
Lung
Msr1-/-
Wild type
0
10
20
30
40
Msr1/Actin (Relative)
b
Percent survival
Msr1-/-
P=0.001
WT
Time after infection (day)
c
Msr1-/-
WT
d
WT
Msr1+/-
Msr1-/-
Msr1
Actb
Wild type
Msr1-/-
Disease score
Time after infection (day)
e
Percent survival
Msr1-/-
P<0.01
Msr1+/-
Time after infection (day)
Msr1+/-
Msr1-/-
Disease score
Time after infection (day)

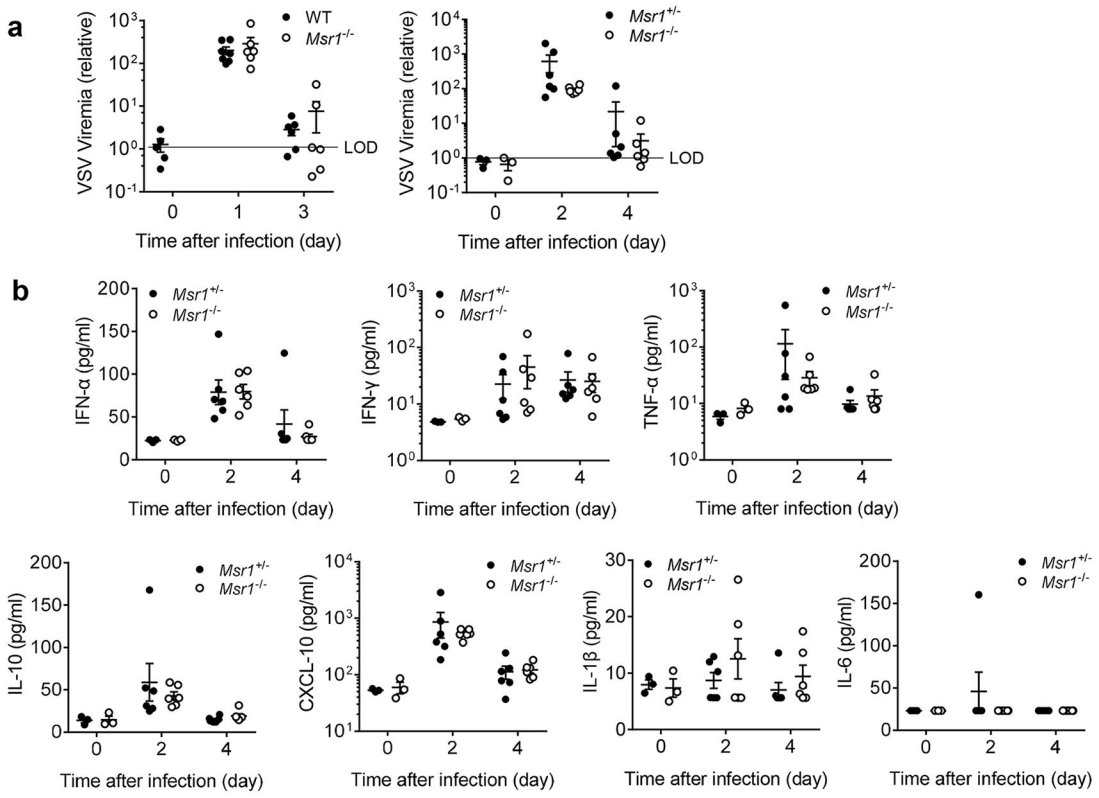
a
VSV Viremia (relative)
WT
Msr1-/-
LOD
Time after infection (day)
Msr1+/-
Msr1-/-
b
IFN-α (pg/ml)
IFN-γ (pg/ml)
TNF-α (pg/ml)
IL-10 (pg/ml)
CXCL-10 (pg/ml)
IL-1β (pg/ml)
IL-6 (pg/ml)
Time after infection (day)

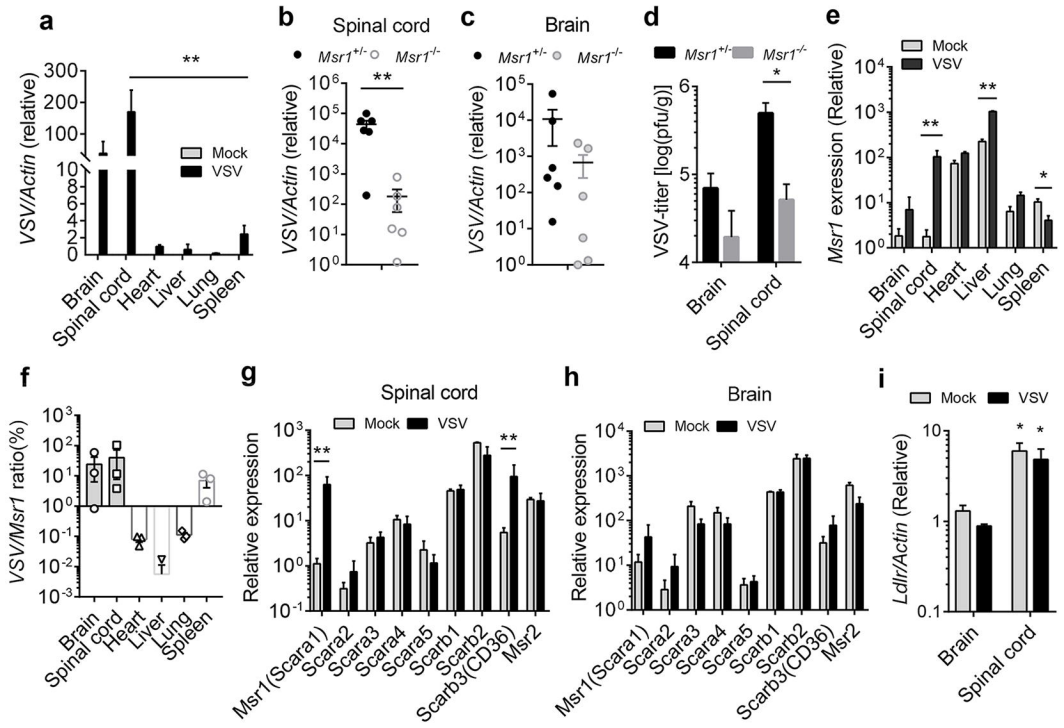
a
VSV/Actin (relative)
Mock
VSV
Brain
Spinal cord
Heart
Liver
Lung
Spleen
b
Spinal cord
Msr1+/-
Msr1-/-
VSV/Actin (relative)
c
Brain
Msr1+/-
Msr1-/-
VSV/Actin (relative)
d
Msr1+/-
Msr1-/-
VSV-titer [log(pfu/g)]
Brain
Spinal cord
e
Mock
VSV
Msr1 expression (Relative)
Brain
Spinal cord
Heart
Liver
Lung
Spleen
f
VSV/Msr1 ratio(%)
Brain
Spinal cord
Heart
Liver
Lung
Spleen
g
Spinal cord
Mock
VSV
Relative expression
Msr1(Scara1)
Scara2
Scara3
Scara4
Scara5
Scarb1
Scarb2
Scarb3(CD36)
Msr2
h
Brain
Mock
VSV
Relative expression
Msr1(Scara1)
Scara2
Scara3
Scara4
Scara5
Scarb1
Scarb2
Scarb3(CD36)
Msr2
i
Mock
VSV
Ldlr/Actin (Relative)
Brain
Spinal cord

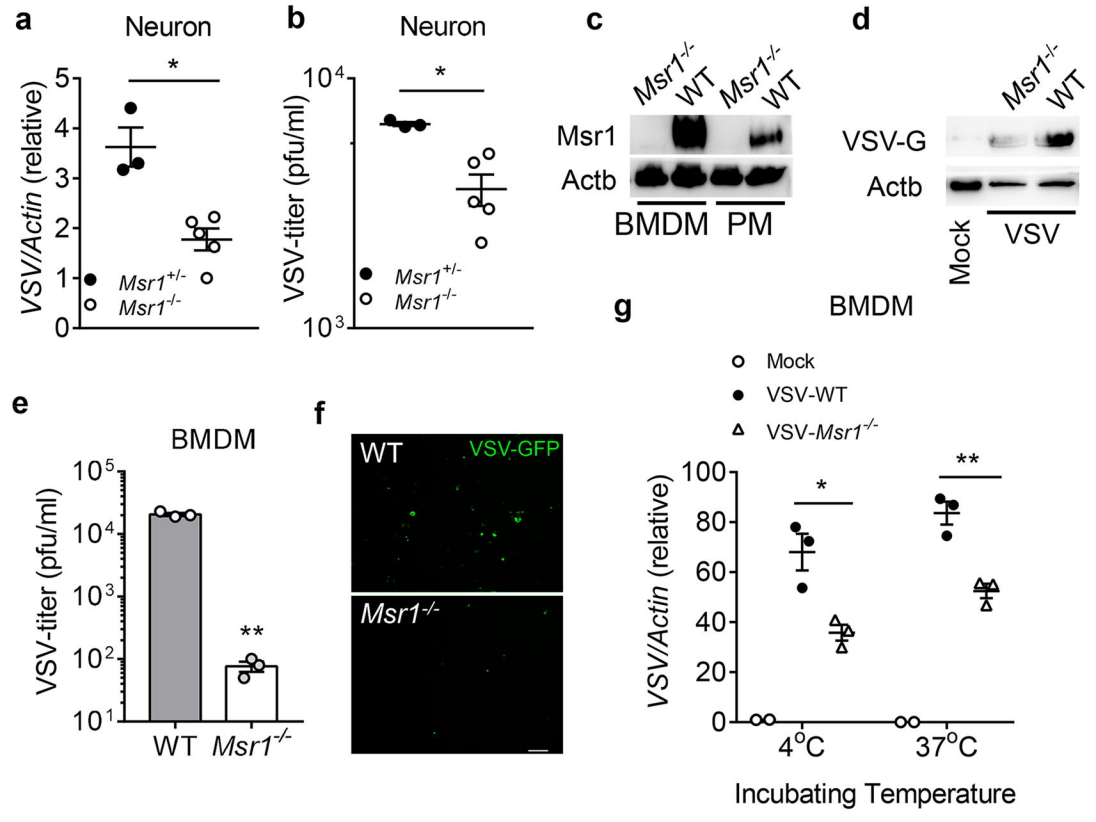
a
Neuron
VSV/Actin (relative)
*
Msr1+/-
Msr1-/-
b
Neuron
VSV-titer (pfu/ml)
*
Msr1+/-
Msr1-/-
c
Msr1-/-
WT
Msr1-/-
WT
Msr1
Actb
BMDM
PM
d
Msr1-/-
WT
VSV-G
Actb
Mock
VSV
e
BMDM
VSV-titer (pfu/ml)
**
WT
Msr1-/-
f
WT
VSV-GFP
Msr1-/-
g
BMDM
Mock
VSV-WT
VSV-Msr1-/-
VSV/Actin (relative)
*
**
4°C
37°C
Incubating Temperature

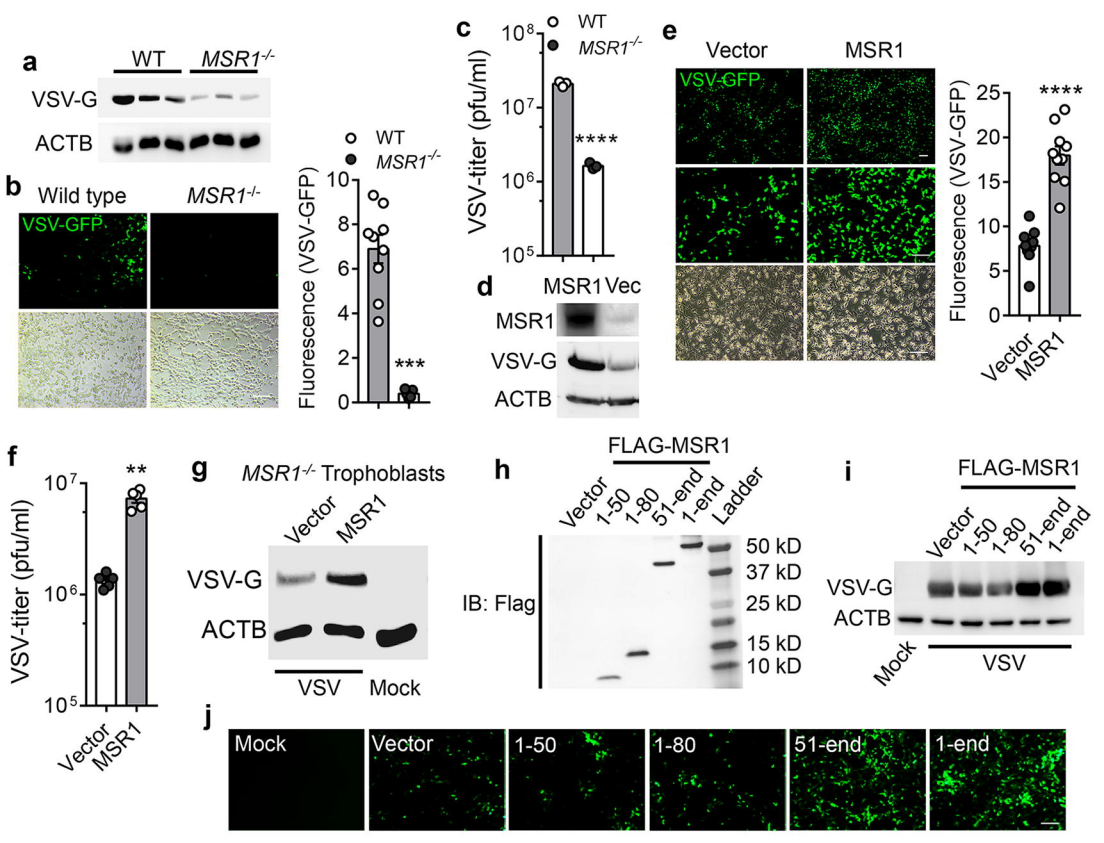
a
WT
MSR1-/-
VSV-G
ACTB
b
Wild type
MSR1-/-
VSV-GFP
WT
MSR1-/-
Fluorescence (VSV-GFP)
***
c
WT
MSR1-/-
VSV-titer (pfu/ml)
****
d
MSR1
Vec
MSR1
VSV-G
ACTB
e
Vector
MSR1
VSV-GFP
Fluorescence (VSV-GFP)
****
Vector
MSR1
f
VSV-titer (pfu/ml)
**
Vector
MSR1
g
MSR1-/- Trophoblasts
Vector
MSR1
VSV-G
ACTB
VSV
Mock
h
FLAG-MSR1
Vector
1-50
1-80
51-end
1-end
Ladder
IB: Flag
50 kD
37 kD
25 kD
15 kD
10 kD
i
FLAG-MSR1
Vector
1-50
1-80
51-end
1-end
VSV-G
ACTB
Mock
VSV
j
Mock
Vector
1-50
1-80
51-end
1-end

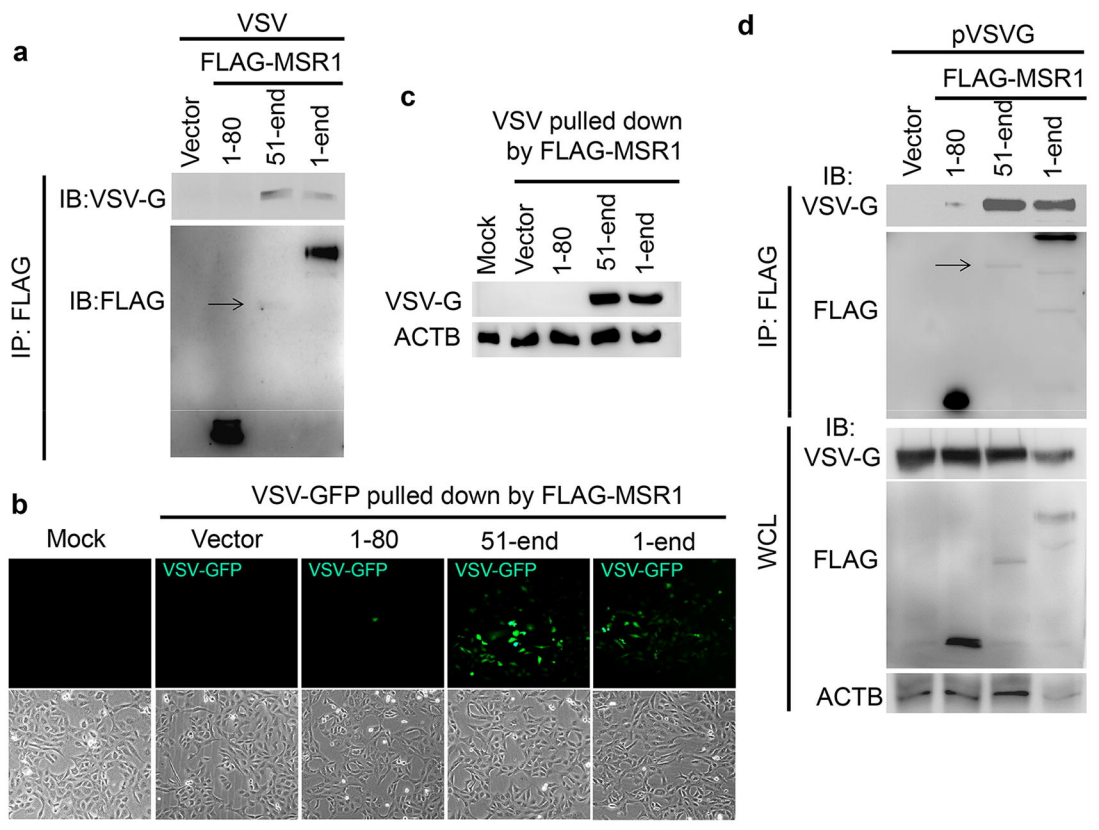
a
VSV
FLAG-MSR1
Vector
1-80
51-end
1-end
IB:VSV-G
IB:FLAG
IP: FLAG
b
VSV-GFP pulled down by FLAG-MSR1
Mock
Vector
1-80
51-end
1-end
VSV-GFP
c
VSV pulled down by FLAG-MSR1
Mock
Vector
1-80
51-end
1-end
VSV-G
ACTB
d
pVSVG
FLAG-MSR1
Vector
1-80
51-end
1-end
IB:
VSV-G
FLAG
IP: FLAG
WCL
ACTB